Dynamic Calorimetry and XRD Studies of the Nematic and Twist-Bend Nematic Phase Transitions in a Series of Dimers with Increasing Spacer Length

Warren D. Stevenson [a,b], Heng-xing Zou [a], Xiang-bing Zeng [b], Christopher Welch [c], Goran Ungar [a,b,*], Georg H. Mehl [c]

[a] Department of Physics, Zhejiang Sci-Tech University, Hangzhou 310018, China
[b] Department of Materials Science and Engineering, University of Sheffield, Sheffield S1 3JD, UK
[c] Department of Chemistry, University of Hull, Hull HU6 7RX, UK

Keywords: N_{tb} phase; twist-bend; helical liquid crystal; modulated DSC; small-angle X-ray diffraction; SAXS; Cybotactic

Abstract:
A modulated and conventional DSC study of the transitions between the twist-bend nematic (N_{tb}), regular nematic (N) and isotropic liquid (Iso) phases was performed on a series of difluoroterphenyl-based dimers with $(CH_2)_n$ spacers; n = 5, 7, 9, 11. The enthalpy of N_{tb}-N transition decreases steeply with increasing n, while that of the N-Iso transition increases with n; hence, the greatest effect of increasing n is a lowering N phase enthalpy. Based on past and present X-ray scattering experiments, we estimate the average molecular conformation in the N_{tb} phase and perform torsion energy calculations on the spacer. From this, the lowering enthalpy of the N phase is attributed to the decreasing torsional energy cost of bringing the two terphenyls from an inclined twisted conformation in the N_{tb} phase, to almost parallel in the N phase. With increasing n the C-C bonds of the spacers twist less away from their *trans* conformation, thereby reducing the overall torsion energy of the N phase. It is speculated that the nearly continuous nature of the N_{tb}-N transition in n=11 dimer is associated with the divergence of the helical pitch toward infinity which is intercepted by a final jump at the very weak (0.01 J/g) first-order transition. Small-angle X-ray scattering results suggest similar local cybotactic layering in both nematic phases, with four sublayers, i.e. tails, mesogens, spacers, mesogens.

The nematic-nematic phase transition has been observed in bent core molecules,[1] trimers,[2-4] larger oligomers[5-7] and main chain polymers,[8-11] but is most frequently reported in achiral liquid crystal (LC) dimers.[12-29] In all of these compounds the adjacent mesogens are angled to each other in a bent conformation, most commonly due to an oligomethylene spacer with an odd number of carbons. The high temperature phase is considered to be the conventional uniaxial nematic (N), where the molecules align preferentially along a common director, although some doubts have been expressed in certain cases. However, in the lower temperature nematic, often referred to as the twist bend nematic (N_{tb}) phase, the local director field is helical, evidenced by a nano-scale pitch length.[12-17] Contrary to the cholesteric phase, the helical director field is not driven by intrinsic chirality, but by closer packing of bent molecular conformations through curvature synchronisation.[30] The molecules tilt in respect to the helical axis in a similar manner to the chiral smectic C (SmC*) phase, but lack long range positional order.[17-20] Moreover, the absence of intrinsic molecular chirality may allow coexistence of both left and right-handed domains.[21-24]

The transition between the N_{tb} and N phases has been the subject of several theoretical treatments, most of which predict a continuous (second order) transition.[31-34] By DSC the transition is observed to be first order in agreement with theories by Katz and Lebadev[35] and also by Lopez et al.[36] In the latter study a phenomelogical Landau model was used to explain experimental findings obtained by modulated DSC (MDSC) of binary dimer mixtures. In the study of weak LC transitions, such as the N_{tb}-N, MDSC has several advantages over standard DSC. Standard DSC only measures net heat flow meaning that first and second order transitions cannot always be distinguished with certainty due to the relatively high heating/cooling rates required to obtain a reasonable signal, meaning that the system is relatively far from equilibrium. MDSC allows much smaller scanning rates to be used, including "pseudoisothermal" experiments. While both DSC and MDSC usually overestimate the enthalpy of LC transitions, there are indications that MDSC produces values much closer to those obtained through adiabatic calorimetry; for example the enthalpy of the N_{tb}-N transition in CBC7CB was measured as 969 J/mol by standard DSC[20] and 205 J/mol by MDSC.[37] The latter is much closer to the 116 J/mol found by adiabatic calorimetry[38] in the closest homologue CBC9CB.

In the present study, MDSC and X-ray diffraction (XRD) were used to investigate the N_{tb}-N transition in a series of difluoroterphenyl-based "DTC5C*n*" dimers with C_5H_{11} end groups and $(CH_2)_n$ spacers, where n = 5, 7, 9, 11. Notably, the latent heat of the N_{tb}-N transition $\Delta H_{Ntb\text{-}N}$ was found to decrease steeply with increasing n and almost

vanishes in DTC5C11, suggesting a divergence of the helical pitch at the transition. In contrast, $\Delta H_{N\text{-}Iso}$ of the nematic-isotropic transition increases markedly with *n*. Thus surprisingly we find a significant drop in enthalpy of the N phase with increasing *n*. Contrary to mean-field models we propose the latter to be due to reduced torsion energy required to straighten dimers with long spacers. The XRD data also provide information on clustering in local layers.

The DTC5C*n* dimers studied in this work are shown in Figure 1a. The synthesis of *n* = 7, 9 and 11 has been described previously in refs 18, 25 and 39, respectively; that of DTC5C5 is provided in the Supporting Information (SI).

In MDSC a linear heating rate is superimposed with a sinusoidal modulation.[40,41] The temperature is then:

$$T(t) = T_0 + vt + \Delta T_M \sin(\omega t) \qquad (1)$$

where T_0 is the starting temperature, v is the linear heating or cooling rate, ω is the angular frequency of the modulation and ΔT_M the modulation amplitude. This gives rise to a modulated heat flow:

$$Q_M(t) = Q_{M0} \cos(\omega t - \phi) \qquad (2)$$

where Q_{M0} is the amplitude and ϕ the phase shift between the temperature modulation and the responding heat flow. The complex heat capacity is thus

$$C_p^*(\omega) = \left(Q_{M0}/\Delta T_M \omega\right) e^{i\phi} \qquad (3)$$

and its real (storage) component

$$C_p'(\omega) = \left(Q_{M0}/\Delta T_M \omega\right) \cos\phi \qquad (4)$$

In instances where the heat flow is reversible, $C_p^* = C_p'$, i.e. $\phi = 0$. However, irreversible heat flow processes, such as those involving latent heat, introduce an additional phase lag ($\phi > 0$) between the set modulated temperature and the responding heat flow. A peak in $\phi(T)$ therefore identifies a first order phase transition.

DSC and MDSC of DTC5C*n* Compounds

All DSC experiments were performed using a TA Instruments Q2000 fitted with a cooling unit and a TZero® high sensitivity cell. Each compound was firstly investigated with linear heating and cooling rates of 3 K/min. The phase sequences of the compounds on heating from the crystal phase are summarised in Table 1. For cooling data see SI. Phase assignments follow from XRD (Figure 2) and microscopy experiments. In addition to the stable smectic (Sm) phase in DTC5C5, metastable lamellar phases were observed on cooling compounds with *n* = 7 and 9. The Sm phases of DTC5C5 and DTC5C7 have the same structure, discussed elsewhere.[39,42] The structure of the Sm phase in DTC5C9 differs and is the subject of further investigation.

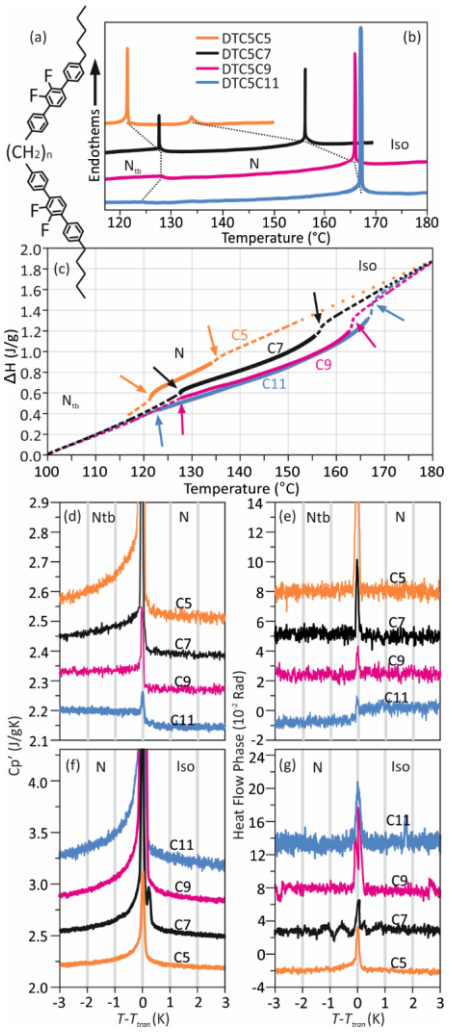

Figure 1 – (a) Chemical structure of DTC5C*n* compounds. (b) Standard DSC heating thermograms (3 K/min) of DTC5C*n* compounds showing N_{tb}-N and N-Iso transitions. Each curve in panels b-f is labelled by spacer length *n*. (c) Temperature dependence of cumulative enthalpy relative to $H_{100°C}$. Bold solid = N phase; arrows indicate transitions. (d) MDSC C_p' curves ±3K of $T_{Ntb\text{-}N}$. (e) Heat flow phase ϕ *vs T* corresponding to (d). (f) MDSC C_p' curves ±3K of $T_{N\text{-}Iso}$. (g) Heat flow phase ϕ *vs T* corresponding to (f). In panels d-f baselines have been shifted for display.

Figure 1b shows that lengthening the spacer reduces $\Delta H_{Ntb\text{-}N}$, while increasing $\Delta H_{N\text{-}Iso}$. The cumulative increase in enthalpy between 100 °C (N_{tb}) and 180 °C (Iso) is displayed in Figure 1c, showing that the main difference between the four compounds is the enthalpy of the N phase, which is reduced significantly with increasing *n*. Enthalpy and entropy values from MDSC experiments are provided in Table 1. This information will be discussed in more detail later. Only a comment here on the disparity between Δ*H* values from standard DSC and MDSC. As mentioned in the Introduction, Δ*H* values from standard DSC are always larger than those from MDSC. The reason is that with the very slow heating rate of MDSC we can separate the transition from pre- and post-transitional heat effects and measure only the true discontinuous enthalpy jump, while with the higher heating rates of standard DSC the clear separation between the continuous and discontinuous enthalpy changes is not possible and a significant portion of the former is included in Δ*H*.

MDSC measurements were performed on DTC5C*n* compounds in the regions of the N_{tb}-N and N-Iso transitions (Figure 1d). The linear heating rate was v = 0.04 K/min, the amplitude ΔT_M = 0.07 K and the modulation frequency ω = 0.31 rad/s (period = 20 s). For DTC5C11 an additional run was recorded with v = 0.01 K/min, but no noticeable difference was observed. Melting of indium and ice where used for temperature calibration, and sapphire for calibration of heat flow.[41] The resulting $C_p'(T)$ and $\phi(T)$ curves close to $T_{Ntb–N}$ and $T_{N\text{-}Iso}$ are displayed in Figures 1d-g.

In all compounds the N_{tb}-N transition endotherm is highly asymmetric, with a very pronounced pretransitional heat absorption on the low-T side (Figure 1d). The largest part of the transition is continuous, with the first-order character becoming extremely weak in DTC5C11. Nevertheless, even a small peak in C_p' (0.01 J/g) accompanied by a small blip in $\phi(T)$ (0.01 rad) are evidence that in fact the transition is still first order. We will discuss this nearly continuous transition further below.

On inspection of Figure 1d one notices the difference between different compounds regarding the shape of the pretransitional $C_p'(T)$: while for n = 5 $C_p'(T)$ increases steeply near $T_{Ntb\text{-}N}$, in compounds with n = 9 and 11 C_p' is temperature-independent though still high near the transition. By contrast, in all four samples there is a sharp post-transitional cut-off in C_p', suggesting that N_{tb} clusters cannot exist beyond $T_{Ntb\text{-}N}$. The asymmetry of the N_{tb}-N peak in LC dimers has already been noted previously,[36,37] and it was also observed in a recent MDSC study of main-chain polymers.[11]

Regarding the N-Iso transition, in all dimers studied here this is clearly marked by a peak in both C_p' and $\phi(T)$. In contrast to the N_{tb}-N transition, the isotropization enthalpy/entropy shows a marked *increase* with *n*. Interestingly in DTC5C5 the N-Iso transition is only weakly first order. Despite considerable pre- and post-transitional increase in C_p, the $\Delta H_{Ntb\text{-}N}$ of the actual discontinuous transition is only 0.17 J/g. Thus for DTC5C5, $\Delta H_{Ntb\text{-}N}$ is actually larger than $\Delta H_{N\text{-}Iso}$.

Table 1 – Transition Temperatures and corresponding Enthalpy and Entropy changes

n	Cr-Sm °C [J/g] (J/molK)	Cr-N_{tb} °C [J/g] (J/molK)	Sm-N_{tb} °C [J/g] (J/molK)	N_{tb}-N °C [J/g] (J/molK)	N-Iso °C [J/g] (J/molK)
5	103.34 [45.5] (89.5)	-	114.74 [2.88] (10.5) *[5.49]	121.59 [0.58] (1.09) *[0.51]	134.01 [0.17] (0.31) *[0.34]
7	-	98.61 [47.5] (98.3)	-	127.47 [0.09] (0.17) *[0.18]	156.57 [0.42] (0.75) *[0.61]
9	-	95.88 [59.1] (127.8)	-	127.91 [0.03] (0.06) *[0.10]	165.81 [0.76] (1.38) *[0.84]
11	-	96.24 [53.1] (118.6)	-	122.55 [0.01] (0.02) *N/A	166.67 [0.86] (1.61) *[1.03]

Enthalpy and entropy measurements of LC transitions from MDSC (0.01-0.04 k/min). Crystal melting from standard DSC (3 K/min). *Transition enthalpies by standard DSC.

X-ray Scattering of DTC5C*n* Compounds

The small and wide angle X-ray scattering (SAXS and WAXS) patterns of the DTC5C*n* compounds were recorded on station BM28 of the ESRF. Samples were sealed in 1.0 mm diameter glass capillaries and placed in a custom heating cell, positioned between the poles of a superconducting solenoid (magnetic field = 2.5T). A helium filled flight tube was positioned between the sample and the Mar165 CCD detector. Each compound was heated into the Iso phase and cooled through its LC transitions.

In the N and N_{tb} phases two broad meridional scattering peaks were observed in the SAXS region, corresponding to $d_1=2\pi/q_1$ and $d_2=2\pi/q_2$ (see Figure 2), where q is the scattered wave vector. In our previous resonant X-ray scattering study[17] it was shown that the two SAXS peaks are always centred in the direction of the N_{tb} helical axis (or director in the N phase). This applies even when the helical axis tilts away from the magnetic field direction at lower temperatures.[17] In the same study it was also shown that the values d_1 and d_2 can be respectively related to the projected dimer length and mesogen separation distance along the helical axis; i.e. $d_1 \approx L\cos(\theta_t)$ and $d_2 \approx M\cos(\theta_t)$. Here θ_t is the tilt angle between the mesogens and helical axis, while L and M are the molecular length

and inter-mesogen separation along the contour of the molecule (discussed later).

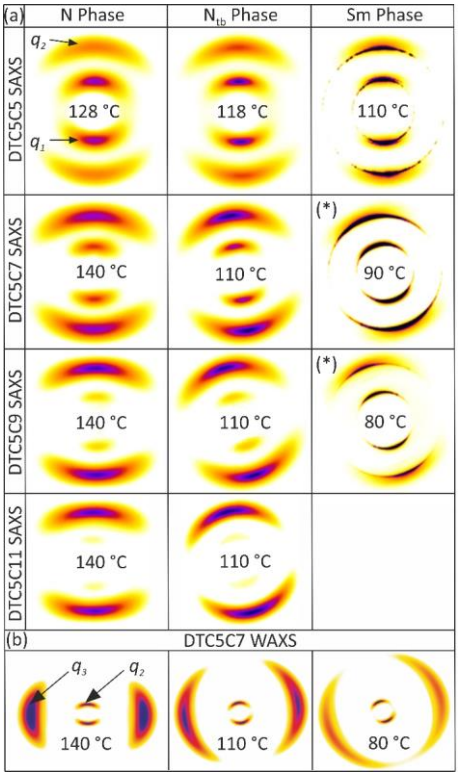

Figure 2 – (a) SAXS and (b) WAXS patterns of magnetically aligned DTC5C*n* compounds in the three LC phases; magnetic field direction is always vertical, B= 2.5T. *Phases only observed on cooling. The WAXS patterns in (b) are of DTC5C7, but appear similar in all compounds.

In the Sm phase the two diffuse SAXS peaks become sharp Bragg reflections. In all three LC phases the WAXS region contains a pair of diffuse equatorial arcs, corresponding to an average side-by-side intermolecular spacing d_3 (=1.117($2\pi/q_3$)) [43]. Comparison of d_3 values in Table 2 shows that the lateral distance between dimers is almost the same for all compounds, and that there is only a marginal increase between N_{tb} and N phases. Like the SAXS peaks, the WAXS arcs tilt and begin to spread azimuthally at lower temperatures. There is a significant increase in azimuthal spread at $T_{N\text{-}Ntb}$, for DTC5C5 (Figure 2b), which is typical for most examples of this transition[17-19] and is due to the developing helical structure of the N_{tb} phase.

For DTC5C*n* compounds the SAXS intensity distribution changes significantly with *n*: q_1 is strong in DTC5C5, but almost invisible in DTC5C11. By measuring the relative intensities, *I(q)*, of the SAXS peaks, the relative structure factors, $F(q_1)$ and $F(q_2)$, were calculated using the relation:

$$F(q) = \sqrt{I(q)}e^{i\psi} \qquad (5)$$

where the phase angle $\psi = 0$ or π was determined by trial and error. From equation (5), the relative electron density along the N_{tb} helical axis, ρ(z), was calculated using a simple lamellar approximation, where $d_1=2d_2$ and

$$\rho(z) = F(q_1)\cos(q_1 z) + F(q_2)\cos(q_2 z) \qquad (6).$$

Table 2 – Summary of SAXS and WAXS Spacings*

n	N Phase			N_{tb} Phase			*L* (nm)	*M* (nm)
	d_1 (nm)	d_2 (nm)	d_3 (nm)	d_1 (nm)	d_2 (nm)	d_3 (nm)		
5	3.9	1.8	0.50	3.8	1.8	0.49	4.6	2.3
7	4.0	1.9	0.51	4.0	1.9	0.51	4.8	2.4
9	4.5	2.1	0.51	4.3	2.0	0.50	5.1	2.5
11	4.8	2.3	0.52	4.8	2.2	0.51	5.4	2.7

**d*-Values measured at temperatures shown in Figure 2; $d_{(1,2)}=2\pi/q_{(1,2)}$, $d_3=1.117(2\pi/q_3)$ [43]. For diffuse SAXS peaks Bragg's law does not strictly apply, meaning $d_{1,2}$ are slight underestimates of the real spacings. The simulated length of the spacer and the combined length of the two end tails were averaged in the calculation of *M*.

Strictly this form of ρ(z) is only applicable to phases with infinite layers, but it is known that in materials exhibiting N_{tb} phase SAXS is generated by short range (cybotactic) layering.[43] As such we believe that the above approximation is valid enough for qualitative discussion. For DTC5C5 and DTC5C11, ρ(z) and its two components are plotted vs *z* in Figure 3a,b. The q_1 contribution (blue dash in 3a,b) progressively reduces with increasing *n* because the spacer and combined length of the two end tails become increasingly similar in length. Notably, the presence of the d_1 SAXS peak means that separation in local layers does not occur only between aromatic and aliphatic moieties, but also between the aliphatic spacers and aliphatic tails. The alternative intercalated model, where spacers and tails are fully mixed, would give ρ(z) equal to the q_2 component alone (red dashed in 3a,b) and the d_1 peak would vanish. The fact that the SAXS patterns of the N and N_{tb} phases are very similar suggests the presence of local layering also in the N phase, but there the conformations do not synchronise to form a helix. This will be revisited later.

Commented [WS1]: I think we should say "short range (cybotactic) layering" or "short range layering (cybotaxis)"

Model and Discussion

The present DSC findings show that increasing the spacer length progressively reduces the energy difference between the N_{tb} and N phases, while simultaneously increasing the energy difference between the N and Iso phases. In the following discussion we explain the variation of $\Delta H_{Ntb\text{-}N}$ and $\Delta H_{N\text{-}Iso}$ in terms of the torsional energy associated with twisting about the spacer bonds, morphing from a curved N_{tb} molecular conformation to a higher energy but straighter conformation, more compatible with N phase.

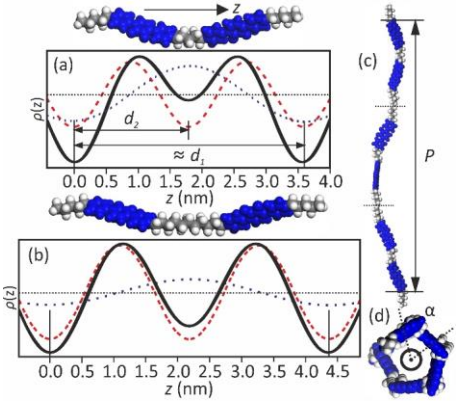

Figure 3 – a,b) Simplified 1D electron density profiles of N_{tb} phase in (a) DTC5C5 and (b) DTC5C11, reconstructed from SAXS intensities along the meridian. Blue/red dashes show separate contributions of q_1/q_2 to ρ(z) (solid black). $\psi = \pi$ for both contributions. The horizontal dotted line is the average electron density. Model molecular conformations matching the density profiles are also shown to aid interpretation. The overlaying molecules have been altered in size to coincide with the d_1=2d_2 lamellar approximation. (c) N_{tb} helix with curved molecular trajectory shown on the example of DTC5C5, P = pitch length. (d) View of (c) along P.

A model of each DTC5C*n* molecule was constructed in Materials Studio (MS), Accelrys, taking a curved helical segment as the N_{tb} conformational average. The models are thought to be applicable to dimers with n = 5 and 7, and to the lower end of the N_{tb} temperature range of dimers DTC5C9 and DTC5C11. The rotation of each successive mesogen around the helical axis was estimated using $\alpha = 2\pi(d_2)/P$, where P represents the N_{tb} helical pitch length (in the bulk). In a dimer mixture ("Se45") consisting of 55% DTC5C7 and 45% of a structurally related seleno-ether, P was measured to vary between 10 and 12 nm, i.e. ≈5.4*d_2 on average.[17] Due to the dependency of P on molecular length and the chemical similarity between DTC5C*n* and Se45, the pitch length of each DTC5C*n* sample was estimated using P≈5.4*d_2, giving α = 67 ° for all four samples. The average exterior bend angle between mesogens (β= 32°) could then be estimated according to $\sin(\beta/2)=\sin(\alpha/2)\sin(\theta_t)$, where θ_t is the average tilt of the mesogens to the helical axis. θ_t was estimated to be 30°, based on previous findings in Se45.[17] To achieve such a twisted conformation (Figures 3a,b and 4a), the torsion angles (γ) of the C-C bonds in the spacer must be moved out of the 180° minimum energy *trans* conformation.

Table 3 – Average Torsional Shifts and Energy Changes between Ntb and Parallel Conformers

n	$\Delta\gamma$ N_{tb} (°)	$\Delta\gamma$ // (°)	e_{Ntb} (kJ/mol)	$e_{//}$ (kJ/mol)	E_{Ntb} (kJ/mol)	$E_{//}$ (kJ/mol)	ΔE (kJ/mol)
5	23.0	42.7	5.2	13.0	20.6	51.8	31.2
7	15.6	25.4	2.5	6.1	15.2	36.6	21.4
9	12.1	17.7	1.6	3.3	12.4	26.6	13.2
11	9.8	14.2	1.0	2.1	10.3	21.1	10.8

//= parallel, $\Delta\gamma$ = average torsional shift from *trans*, e = average torsion energy per bond, $E = e(n\text{-}1)$ = average torsion energy per whole spacer, ΔE = torsional energy difference between N_{tb} and // spacer conformations

If we now consider the N phase, the molecules abandon the helix in favour of straighter conformations. This increases compatibility with a linear director and increases translational freedom. However, in all four compounds the *d*-values barely change between the two nematic phases, suggesting that the local packing and θ_t of the mesogens stay roughly the same. To straighten the conformation, the molecules must reduce the bend β by reducing γ values, i.e. by twisting the spacer C-C bonds even further away from the *trans* state; this extra twisting must carry a torsional energy penalty. In the following we explore the torsional energy difference between the predicted N_{tb} conformation and an idealised N phase conformation with the two mesogen arms parallel (parallel conformation, Figure 4b). The parallel conformation represents the upper limit of torsional energy, but in reality we expect the average N phase conformer to remain somewhat bent, requiring lower energy than this maximum.

The helical N_{tb} and parallel N conformations of the four dimers, such as those in Figure 4, were built using the Forcite module of MS (Universal Force Field). For the N_{tb} calculation, the C-C bonds of each DTC5C*n* spacer were rotated equally to produce the estimated values of helical rotation α and bend angle β between mesogens. Energy minimisation was then performed, keeping mesogens fixed, but allowing the spacer to equilibrate. Similar calculations have been performed previously by Mandle and coworkers[44,45] but in those cases conformational probability, or "landscape", was explored rather than the energy

difference between two predetermined configurations. Our calculations assumed a sinusoidal torsion potential comparable to that of butane,[46] i.e. *trans* (γ=180°) = 0 kJ/mol and eclipsed (γ=120°) = 16 kJ/mol. An identical calculation was performed for the parallel conformation, but with the mesogens fixed parallel. The average rotational shift of the C-C bonds from the *trans* state, Δγ (=180°-⟨γ⟩), and the values of the total torsional energy E_{Ntb} and $E_{//}$ of the minimised spacer, are provided for both conformers in Table 3. The data show that both E_{Ntb} and $E_{//}$ reduce with increasing *n*, as does their difference ΔE. This is because the average torsion energy per rotatable C-C bond of the spacer, $e(\Delta\gamma) = E/(n\text{-}1)$, has a sinusoidal rather than linear dependence on Δγ. Thus, e.g., for *n* = 11 and 5, $10e(\Delta\gamma_{11}) << 4e(\Delta\gamma_5)$ for relatively small Δγ. Increasing *n* spreads the twist over more bonds, allowing Δγ of each bond to remain close to the trough of the sinusoidal potential, requiring low *e* and a low overall *E*. The reducing $\Delta H_{Ntb\text{-}N}$ with increasing *n* is thus related to the decreasing energy difference Δ*E* between the parallel and helical molecular conformations, as listed in the last column of Table 3.

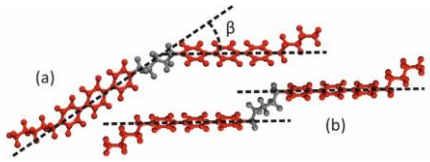

Figure 4 – (a) Estimated N_{tb} conformation with β = 32°; this produces α = 67° when tilted 30° to the helical axis. Shown at a different angle to Figure 3a. (b) Parallel conformation representing torsional maximum.

The increasing enthalpy of the N-Iso transition with increasing *n* can accordingly be explained again by reference to Figure 1c and Table 3. In long spacer compounds the low conformational cost of the nematic phase (parallel conformation) means that eventually, at the N-Iso transition, the enthalpy must catch up with that of the other compounds, requiring large heat absorption. On the other hand, for the short-spacer dimers, most of the heat absorption that would be typically associated with isotropization is already spent on bond torsion in the N phase. Thus a large part of the heat of isotropization is compensated for by heat release due to relaxation of torsional strain, as "straightness" due to the nematic director field is no longer required. In the isotropic the C-C bonds can assume γ's corresponding to *trans* and *gauche* energy minima; this energy compensation results in near vanishing of $\Delta H_{N\text{-}Iso}$ in DTC5C5 (Figure 1).

We note that a similar argument can also be applied to explaining the dependence of isotropization temperature $T_{N\text{-}Iso}$ on *n*. E.g. the significant increase in $T_{N\text{-}Iso}$ of DTC5C7 relative to that of DTC5C5 (Figure 1c and Table 1) can be attributed to the lower torsional energy and thus higher stability of the N phase of DTC5C7.

Returning to the N_{tb}-N transition there is a pronounced pre-transitional upswing in C_p' (Figure 1d) meaning that a significant part of the conformational change, i.e. the straightening of the dimer, occurs continuously with increasing temperature. We believe that this continuously decreasing molecular bend is responsible for the increasing N_{tb} pitch length with temperature, observed by resonant X-ray scattering.[15-17] In the case of the very weakly first order N_{tb}-N transitions such as in DTC5C11 it would therefore be expected that the helical pitch continuously diverges toward infinity, interrupted only at a high pitch length with a final jump to infinity at $T_{Ntb\text{-}N}$.

Finally it is interesting to compare our results with those by Lopez at al.[36] who studied binary mixtures of an asymmetric di-ether dimer FFO9OCB and the "classic" symmetric cyanobiphenyl dimer CBC7CB; the two differ in length, flexibility and molecular curvature. MDSC measurements showed that decreasing the percentage of CBC7CB in the mixture decreased $\Delta H_{Ntb\text{-}N}$ and widened the N phase temperature range. In explanation of these findings a mean field Landau model was proposed comparable to that of Katz and Lebadev,[35] where the transition occurs at finite helical pitch length and involves two order parameters: a nematic orientational order parameter and a rotational vector field relating to the conical angle. In the version by Lopez et al. the resulting free energy density depends largely on the effective value of the twist Frank elastic constant K_{2eff}, which takes a negative value in the N_{tb} phase and increases with temperature. This first order transition model has been shown to produce good fits to experimental DSC data in N_{tb} dimers.[36-47] Although there has been success with mean field models, our present findings show that $\Delta H_{Ntb\text{-}N}$ and $\Delta H_{N\text{-}Iso}$ are related directly to a molecular feature, the spacer length. While increasing the spacer length does change the molecular length and curvature, we believe that the most important thing changing here is molecular flexibility. Referring back to the work by Lopez et al., FFO9OCB, containing two ether links, is more flexible than CBC7CB and so decreasing the percentage of CBC7CB in mixtures serves to increase average flexibility, meaning their findings can also be explained in these terms.

Summary

MDSC and SAXS/WAXS were used to investigate the N_{tb}-N and N-Iso transitions in a series of bent dimers with varying spacer length. MDSC revealed that Δ*H* of the N_{tb}-N transition decreases dramatically with increasing number of carbons *n* in the spacer, the transition remaining only weakly first order for *n*=11. At the same time the enthalpy and temperature of the N-Iso transition increase *with n*. Thus surprisingly the main effect of lengthening the spacer is to lower the enthalpy of the N phase. This is attributed to lower C-C torsion angles and torsion energies in long spacers required to keep the molecules straight in the nematic phase.

SAXS and the reconstructed electron density suggest local layering in both the N_{tb} and N phases, with spacers and terminal chains segregated in separate aliphatic layers. For future work, the proposed divergence of the helical pitch $P(T)$, with $P \rightarrow \infty$ at N_{tb}-N transition in a dimer such as DTC5C11, should be tested using resonant XRD. Additionally, theory developments involving order parameters dependent on the twist/bend between mesogens, rather than tilting angle,[31] may be advantageous.

Acknowledgements

We would like to thank Drs. O. Bikondoa, S. Brown and P. Thompson at beamline BM28 of ESRF. We acknowledge funding from EPSRC (EP-P002250 and EP/M015726/1) and from the 1000 Talents program of the Government of China.

1. D. Chen, M. Nakata, R. Shao, M. R. Tuchband, M. Shuai, U. Baumeister, W. Weissflog, D. M. Walba, M. A. Glaser, J. E. Maclennan, N. A. Clarke, *Phys. Rev. E*, 2014, **89**, 022506.
2. Y. Wang, G. Singh, D. M. Agra-Kooijman, M. Gao, H. K. Bisoyi, C. M. Xue, M. R. Fisch, S. Kumar, Q. Li, *CrystEngComm*, 2015, **17**, 2778.
3. S. M. Jansze, A. Martínez-Felipe, J. D. M. Storey, A. T. M. Marcelis, C. T. Imrie, *Angew. Chem. Int. Ed*., 2015, **54**, 643.
4. C. Welch, W. D. Stevenson, X. B. Zeng, G. Ungar, G. H. Mehl, (in preparation).
5. R. J. Mandle, J. W. Goodby, *ChemPhysChem*, 2016, **17**, 967.
6. R. J. Mandle, J. W. Goodby, *RSC Adv.*, 2016, **6**, 34885.
7. F. Simpson, R. J. Mandle, J. N. Moore, J. W. Goodby, *J. Mater. Chem. C*, 2017, **5**, 5102.
8. G. Ungar, J. L. Feijoo, A. Keller, R. Yourd, V. Percec, *Macromolecules*, 1990, **23**, 3411.
9. G. Ungar, V. Percec, M. Zuber, *Macromolecules*, 1992, **25**, 75.
10. G. Ungar, V. Percec, M. Zuber, *Polym. Bull.*, 1994, **32**, 1325.
11. W. D. Stevenson, J. An, X. B. Zeng, M. Xue, H.-X. Zou, Y.-S. Liu, G. Ungar, *Soft Matter*, 2018, **14**, 3003.
12. D. Chen, J. H. Porada, J. B. Hooper, A. Klittnick, Y. Shen, M. R.Tuchband, E. Korblova, D. Bedrov, D. M. Walba, M. A. Glaser, J. E. Maclennan, N. A. Clark, *Proc. Natl. Acad. Sci. U.S.A.*, 2013, **110**, 15931.
13. J. W. Emsley, M. Lelli, G. R. Luckhurst, H. Zimmermann, Phys. Rev. E 2017, **96**, 062702.
14. E. Gorecka, M. Salamończyk, A. Zep, D. Pociecha, C. Welch, Z. Ahmed, G. H. Mehl, *Liq. Cryst.*, 2015, **42**, 1.
15. C. Zhu, M. R. Tuchband, A. Young, M. Shuai, A. Scarbrough, D. M. Walba, J. E. Maclennan, C. Wang, A. Hexemer, N. A. Clark, *Phys. Rev. Lett.*, 2016, **116**, 147803.
16. M. Salamończyk, N. Vaupotič, D. Pociecha, C. Wang, C. Zhu, E. Gorecka, *Soft Matter*, 2017, **13**, 6694
17. W. D. Stevenson, Z. Ahmed, X. B. Zeng, C. Welch, G. Ungar, G. H. Mehl, *Phys. Chem. Chem. Phys*., 2017, **19**, 13449.
18. V. Borshch, Y.-K. Kim, J. Xiang, M. Gao, A. J´akli, V. P. Panov, J. K. Vij, C. T. Imrie, M. G. Tamba, G. H. Mehl, O. D. Lavrentovich, *Nat. Commun*., 2013, **4**, 2635.
19. K. Adlem, M. Čopič, G. R. Luckhurst, A. Mertelj, O. Parri, R. M. Richardson, B. D. Snow, B. A. Timimi, R. P. Tuffin, D. Wilkes. *Phys. Rev. E*, 2013, **88**, 022503.
20. M. Cestari, S. Diez-Berart, D. A. Dunmur, A. Ferrarini, M. R. de la Fuente, D. J. B. Jackson, D. O. López, G. R. Luckhurst, M. A. Perez-Jubindo, R. M. Richardson, J. Salud, B. A. Timimi, and H. Zimmermann, *Phys. Rev. E*, 2011, **84**, 031704.
21. L. Beguin, J. W. Emsley, M. Lelli, A. Lesage, G. R. Luckhurst, B. A. Timimi, H. Zimmermann, *J. Phys. Chem. B*, 2012, **116**, 7940.
22. C. Meyer, G. R. Luckhurst, I. Dozov, *J. Mater. Chem. C*, 2015, **3**, 318.
23. C. Meyer, G. R. Luckhurst, I. Dozov, *PRL*, 2013, **111**, 067801.
24. V. P. Panov, R. Balachandran, M. Nagaraj, J. K. Vij, M. G. Tamba, A. Kohlmeier, G. H. Mehl, *App. Phys. Lett.*, 2011, **99**, 261903.
25. V. P. Panov, M. Nagaraj, J. K. Vij, Y. P. Panarin, A. Kohlmeier, M. G. Tamba, R. A. Lewis, G. H. Mehl, *Phys. Rev. Lett*, 2010, **105**, 167801.
26. Z. Zhang, V. P. Panov, M. Nagaraj, R. J. Mandle, J. W. Goodby, G. R. Luckhurst, J. C. Jones, H. F. Gleeson, *J. Mater. Chem. C*, 2015, **3**, 10007.
27. A. Hoffmann, A. G. Vanakaras, A. Kohlmeier, G. H. Mehl, D. J. Photinos, *Soft Matter*, 2015, **11**, 850.
28. P. K. Challa, V. Borshch, O. Parri, C. T. Imrie, S. N. Sprunt, J. T. Gleeson, O. D. Lavrentovich, A. Jákli, *Phys. Rev. E*, 2014, **89**, 060501.
29. C. Greco, G. R. Luckhurst, A. Ferrarini, *Phys. Chem. Chem. Phys.*, 2013, **15**, 14961.
30. I. Dozov, *Europhys. Lett.*, 2001, **56**, 247.
31. A. Matsuyama, *J. Phys. Soc. Jpn.*, 2016, **85**, 114606.
32. S. M. Shamid, S. Dhakal, J. V. Selinger, *Phys. Rev. E*, 2013, **87**, 052503.
33. G. Barbero, L. R. Evangelista, M. P. Rosseto, R. S. Zola, I. Lelidis, *Phys. Rev. E*, 2015, **92**, 030501(R).

34. C. Greco, G. R. Luckhurst, and A. Ferrarini, *Soft Matter*, 2014, **10**, 9318.
35. E. I. Katz, V. V. Lebedev, *JETP Letters*, 2014, **100**, 110.
36. D. O. López, B. Robles-Hernández, J. Salud, M. R. de la Fuente, N. Sabastián, S. Diez-Berart, X. Jaen, D. A. Dunmur, G. R. Luckhurst, *Phys. Chem. Chem. Phys*., 2016, **18**, 4394.
37. B. Robles-Hernández, N. Sabastián, M. R. de la Fuente, D. O. López, S. Diez-Berart, J. Salud, M. B. Ros, D. A. Dunmur, G. R. Luckhurst, B. A. Timimi, *Phys. Rev. E*, 2015, **92**, 062505.
38. A. Kohlmeier, M.-G. Tamba, G. H. Mehl, *Phys. Rev. E*, 2011, **84**, 041707.
39. M. G. Tamba, S. M. Salili, C. Zhang, A. Jákli, G. H. Mehl, R. Stannarius, A. Eremin. *RCS Adv.*, 2015, **5**, 11207.
40. M. B. Sied, J. Salud, D. O. Lopez, M. Barrio J. L. Tamarit, *Phys. Chem. Chem. Phys.*, 2002, **4**, 2587.
41. I. Hatta, S. Muramatsu, Jpn. J. Appl. Phys. 1996, 35 L858.
42. N. Sebastián, M. G. Tamba, R. Stannarius, M. R. de la Fuente, M. Salamonczyk, G. Cukrov, J. Gleeson, S. Sprunt, A. Jákli, C. Welch, Z. Ahmed, G. H. Mehl, A. Eremin, *Phys. Chem. Chem Phys.*, 2016, **18**, 19299.
43. A. de Vries, Mol. Cryst. Liq. Cryst, 1970, 10, 219.
44. R. J. Mandle, *Chem. Eur. J.*, 2017, **23**, 8771.
45. A. Lesac, U. Baumeister, I. Dokli, Z. Hameršak, T. Ivšić, D. Kontrec, M. Viskić, A. Kneževića R. J. Mandle, *Liq. Cryst.* 2018, **45**, 1101-1110.
46. J. Claydon, N. Greeves, S. Warren, P. Wothers, "*Organic Chemistry*", 2001, Oxford University Press, New York, USA.
47. D. A. Paterson, M. Gau, Y.-K. Kim, A. Jamali, K. L. Finley, B. Robles-Hernández, S. Diez-Berart, J. Salud, M. R. de la Fuente, B. A. Timimi, H. Zimmermann, C. Greco, A. Ferrarini, J. M. D. Storey, D. O. López, O. D. Lavrentovich, G. R. Luckhurst, C. T. Imrie, *Softmatter*, 2016, **12**, 6827.